Mikhailova, O., del Campo, A., Rovnanik, P., Fernández, J. & Torres-Carrasco, M. (2019). In situ characterization of main reaction products in alkali-activated slag materials by Confocal Raman Microscopy. *Cement and Concrete Composites, 99*, 32–39.

DOI: 10.1016/j.cemconcomp.2019.02.004

In situ characterization of main reaction products in alkali-activated slag materials by Confocal Raman Microscopy

O. Mikhailova[1], A. del Campo[2], P. Rovnanik[1], J.F. Fernández[2] and M. Torres-Carrasco[2*]

[1]Brno University of Technology, Faculty of Civil Engineering, Chemistry Department, Brno, Czech Republic

[2]Ceramic and Glass Institute (ICV-CSIC), Madrid, Spain

*Corresponding author: mtorres@icv.csic.es

Abstract

The re-use of different aluminosilicates, such as blast furnace slag, in the preparation of alternative binders (alkali-activated materials) to Portland cement materials is well document and evaluated by conventional techniques. The use of XRD, FTIR and TG techniques allows obtaining information about the hydration products formed under the conditions of alkaline activation. The formation of the main reaction product (C-A-S-H gel), due to its low crystallinity, is not easily stablished by XRD or FTIR, and it is also quite complex to obtain quantitative information. Confocal Raman Microscopy (CRM) technique reveals information of each of the present phases during the slag activation and in particular. Moreover, CRM provide the evolution of C-A-S-H gel confirming that the growth of the C-A-S-H gel in activate alkaline-systems is different from that an Ordinary Portland Cement system. C-A-S-H gel grows randomly in the regions rich in calcium and silicon. The use of CRM opens a new possibility for the in situ study of complex systems such as the activation of alkali-activated or geopolymers in the search for alternative materials to Portland cement.

Keywords: alkali activated slag; Confocal Raman Microscopy (CRM); C-A-S-H gel; characterization

1. Introduction

The production of Ordinary Portland Cement (OPC) it is associated with a high energy consumption and with greenhouse gas emissions [1]. The manufacturing of 1 ton of cement leads to approximately 0.94 tons of CO_2 emitted into the atmosphere [2]. Moreover, the OPC production requires overexploitation of quarries that have a

significant impact on the landscape pollution. Hence, the development of new cementitious materials alternative to traditional Portland cement is a technological challenge that in recent years has attracted the scientific interest. One of the focuses of attention in an alternative to OPC is the alkali-activated materials (AAM) or geopolymers due their enormous potential [3]. Industrial by-products such as granulated blast furnace slag (derived from the steel making industry), fly ash or metakaolin are used as the main precursors for the production of alkali-activated materials among others [4,5]. By using this type of precursors, in addition to generating new alternative materials to Portland cement, it is favoring the circular economy of different industrial by-products, which, otherwise, would end up in landfills. Alkali-activated materials compared to cement materials have the following features: lower heat of hydration [6]; the development of earlier and higher mechanical properties [7]; better resistance against chemical attack [8–10]; freeze-thaw resistance [11]; fire resistance [12]; higher reduction in chloride diffusion [11,13]; and stronger aggregate-matrix interface formation [14,15].

The main reaction product formed in OPC concrete is C–S–H gel, which greatly influence the strength, durability, and other physical and chemical properties of hydrated OPC [16]. In materials with high calcium content, such as blast furnace slag, activation generates reaction products that resemble the products precipitating during OPC hydration. The main reaction product is a silicoaluminate calcium hydrate gel ($CaO(\text{-}Al_2O_3)\text{-}SiO_2\text{-}H_2O$), commonly called C-A-S-H gel that confers high mechanical properties of the material [17,18]. A number of secondary products may form, including hydrotalcite and calcite, depending on activator type and concentration, slag structure and composition, and the curing conditions under which the paste hardens [19].

C-A-S-H gels can be regarded as a new phase of aluminum in the C-S-H structure gel and it is the principal binding phase in hardened OPC pastes and concretes. It is generally believed that the C-A-S-H gels and the C-S-H gels have a similar tobermorite structure [20,21]. However, the low-crystallinity of the C–A–S–H phase is a limiting factor to study their formation reaction. Their structure, the effects of Ca, Si and Al cations in the reactivity and the microstructure of the alkali activated binder have been evaluated by several characterization techniques, such as X-ray diffraction (XRD) [4,22], Fourier Transform infrared spectroscopy FTIR [4,23], differential thermal

analysis (DTA), thermogravimetry (TG), NMR ^{29}Si and ^{27}Al [24] and Raman spectroscopy [25,26].

In 1970s, Bensted first showed that it was possible to obtain Raman spectra from cement materials [27]. During the last years there has been an evolution in the use of Raman spectroscopy in the study of hydrated and anhydrous cement phases [24,26–30]. Ortaboy at al. [31] recently investigated the structure and chemistry of C–A–S–H by Raman spectroscopy. They proved that the incorporation of aluminum in the C–S–H structures causes the formation of different types of aluminum species depending on the Ca content of the sample. Also it was confirmed that increasing synthesis temperature and aluminum content in C–A–S–H promote the formation of an 11 Å tobermorite-like structure. However, as cementitious based materials combined several phases the correlation of Raman spectra with the microstructure is a challenge.

In recent years Confocal Raman Microscopy (CRM) has become a new technique to determine structural characterization of C–S–H phases due to its molecular sensitivity. Confocal Raman microscopy refers to the ability to analyze samples in the XY (lateral) and Z (depth) axes. Few articles describing about this method for determine C-S-H in OPC systems [32–34]. In 2013 Schmid et al.[34] firstly succeed to demonstrate the potential of Raman imaging of historical cements. Higl et al. [32] proved that CRM technique can be used for microstructural characterization of hydrating cementations pastes at early age. In addition, Torres-Carrasco et al. [33] used the Confocal Raman Microscopy to determine the weathering of commercial cement. CRM can show the presence and distribution of the main phases present in cementitious based materials.

The present work deals with the application of Raman spectroscopy to the study of C-A-S-H systems in alkali activated materials and to introduce Confocal Raman Microscopy as a promising novel technique for microstructural characterization of hydrating alkali activated materials. Moreover, with the use of CRM is possible to obtain, apart from the spectral signature, the distribution (Raman imaging) of the reaction products through reaction time and information on both the solid precursor (in this case blast furnace slag) and the alkaline activator (liquid, waterglass solution) used during alkaline activation.

2. Experimental procedure

2.1. Materials

In this study Czech ground-granulated blast-furnace slag (Kotouč Štramberk, spol. s r.o.) was used as the primary precursor. The chemical composition of slag is given in Table 1. The specific surface of the slag was 380 m^2/kg. The particle size range, determined through laser granulometry, was d_{50} = 19 µm. The commercial solid sodium water glass SUSIL (27% SiO_2; 8% Na_2O and 65% H_2O by weight) with a SiO_2/Na_2O ratio of 2.0 was used as alkaline activator. Alkali-activated slag (AAS) pastes with a L/S ratio 0.32 were prepared. AAS pastes samples were chamber-cured (99% relative humidity, 20 ± 2ºC) for 1, 2, 7 and 28 days. The sample pastes were treated with acetone/ethanol to detain hydration/activation [35].

Table 1. Chemical analysis of blast furnace slag determined by FRX (expressed as equivalent oxides, %)

wt. %	**CaO**	**SiO_2**	**Al_2O_3**	**MgO**	**Fe_2O_3**	**Na_2O**	**K_2O**	**MnO**	**Cl**	**SO_3**	***LoI**
Slag	40.12	39.66	6.45	9.5	0.47	0.33	0.55	0.65	0.05	0.72	1.25

2.2. Techniques of characterization

FRX. A Philips PW-1004 X-ray spectrometer was used, with a Sc-Mo X-ray generator tube. Before analyzing the starting materials by FRX, the weight loss thereof was quantified after a heat treatment of 1 hour at 1000ºC.

Particle size distribution of blast furnace slag was evaluated by an analyzer Helos 12K of Sympatec mark. Samples were analyzed suspended in isopropyl alcohol with an ultra-sonic time of 60 s and measurement time of 15 s.

Specific surface area from **BET method** was found from nitrogen adsorption isotherm generated by a Micromeritics ASAP 2010 analyzer.

X-ray diffraction (XRD). The XRD patterns for the samples were recorded on a Bruker AXS D8 Advance diffractometer fitted with a Lynxeye super speed RX detector, a 2.2-kW Cu anode and no monochromator. The scanning range, from 5 to 60º, was covered in a 24-minute period. The instrument was set at 40 kW and 30 mA and the sample was not rotated during scanning.

FTIR. Fourier Transform Infrared spectroscopy (FTIR) of samples was carried out by FTIR spectrometer Perkin Elmer, Spectrum 100, with a spectral resolution of 2 cm^{-1} in the frequency mode range of 400-4000 cm^{-1}.

Thermogravimetric analysis (TG). The TG test was performed by using an adaption of the ASTM E1131:2008 standard, on thermogravimetric and compositional analysis of solid and liquids. The equipment used was the simultaneous thermal analyser Setaram brand, model Labsys Evo with a balance accurate to 0.1 mg. The dynamic heating ramp varied between 40ºC and 800ºC. The heating rate was 10ºC/min and the crucibles used were made of alumina. The reference material was α-alumina (α-Al_2O_3). The test was conducted under N_2 atmosphere. All the tests were performed by using approximately 50 mg of previously ground sample.

Confocal Raman microscopy (CRM). Confocal Raman measurements have been accomplished using a 532 nm excitation laser (green laser) and a 100X objective lens (N.A. 0.95) with and area of focus over the sample at a 20 mW laser power (Witec alpha 300R, Witec, Ulm, Germany). All measurements were carried out in the samples to identify the modification of each of the phases present in the anhydrous blast furnace slag and in the new phases formed after the activation with sodium silicate hydrate. Collected Raman spectra were analyzed by using Witec Control Plus Software (Witec, Ulm, Germany). For the treatment of the results obtained by Confocal Raman microscopy, "cosmic rays remove" (CRR) and "background subtraction" (BSub) were performed.

3. Results and discussion

3.1. Classical determination of the main reaction products: FTIR, XRD and TG.

In Figure 1a FTIR spectra of the anhydrous slag is presented. The absorption band ca. 930 cm^{-1} in the anhydrous slag is related to the Si-O vibration band generated by the SiO_4 groups [36]. In addition, the absorption band ca. 508 cm^{-1} is associated to v_4 [Si-O-Si] bonds vibrations, and the absorption band ca. 669 cm^{-1} is due to the stretching vibrations generated by the Al-O bonds in the AlO_4 groups [37]. The presence of carbonate in this material is evident. The band at ca. 1420 cm^{-1} is attributed to the asymmetric tension vibrations of the C-O bonds of the CO_3^{2-} (v_3) group, and the sharp and strong absorption band around 874 cm^{-1} is characteristic of the vibration of

deformation of O-C-O bonds out of the plane (v_2), which indicates the presence of calcite [38,39]. The presence of a high content of calcium in the chemical composition causes that there is a carbonation form the beginning of the slag.

Figure 1a shows the FTIR spectra of AAS pastes activated at 1, 2, 7 and 28 days. It is observed that as the reaction time evolves with time, there is a slight displacement of the main absorption band (related to the Si-O-Si vibrations) towards higher wavenumbers, as a result of the formation of calcium silicoaluminate hydrated compound, C-A-S-H gel (see Figure 1b). This shift towards higher wavelengths of the main absorption band is typical of alkali activated slag pastes with silicon rich solutions, so that the gel that will be formed will be much richer in silicon, without becoming a silica gel [40]. The absorption band that appears ca. 450 cm^{-1} (in the anhydrous slag appeared ca. 508 cm^{-1}) is assigned to the vibrations of δ Si-O-Si bonds, v_4, due to the formation of the C-A-S-H gel, while the absorption band observed ca. 669 cm^{-1} is due to the Al-O vibrations of the AlO_4 groups (see Figure 1c). The FTIR spectra also contain absorption bands at ca. 1420 cm^{-1} attributed to CO_3^{2-}, v_3, confirming the carbonation or weathering of the pastes.

The v_{as} located ca. 967 cm^{-1}, shows an intensity decreasing in comparison with the compared to the Si-O-Si bonds of anhydrous blast furnace slag. This effect is related to the incorporation of aluminum and calcium to the Si-O chains to form the main reaction product (C-A-S-H gel). As identified by Garcia-Lodeiro et al. [41,42], the displacement of sodium by calcium in the (N,C)-A-S-H gels does not imply relevant changes in the position of the absorption band, but the variation in its shape is a possible sign of the precipitation of new phases that are not typical components of C-S-H gels.

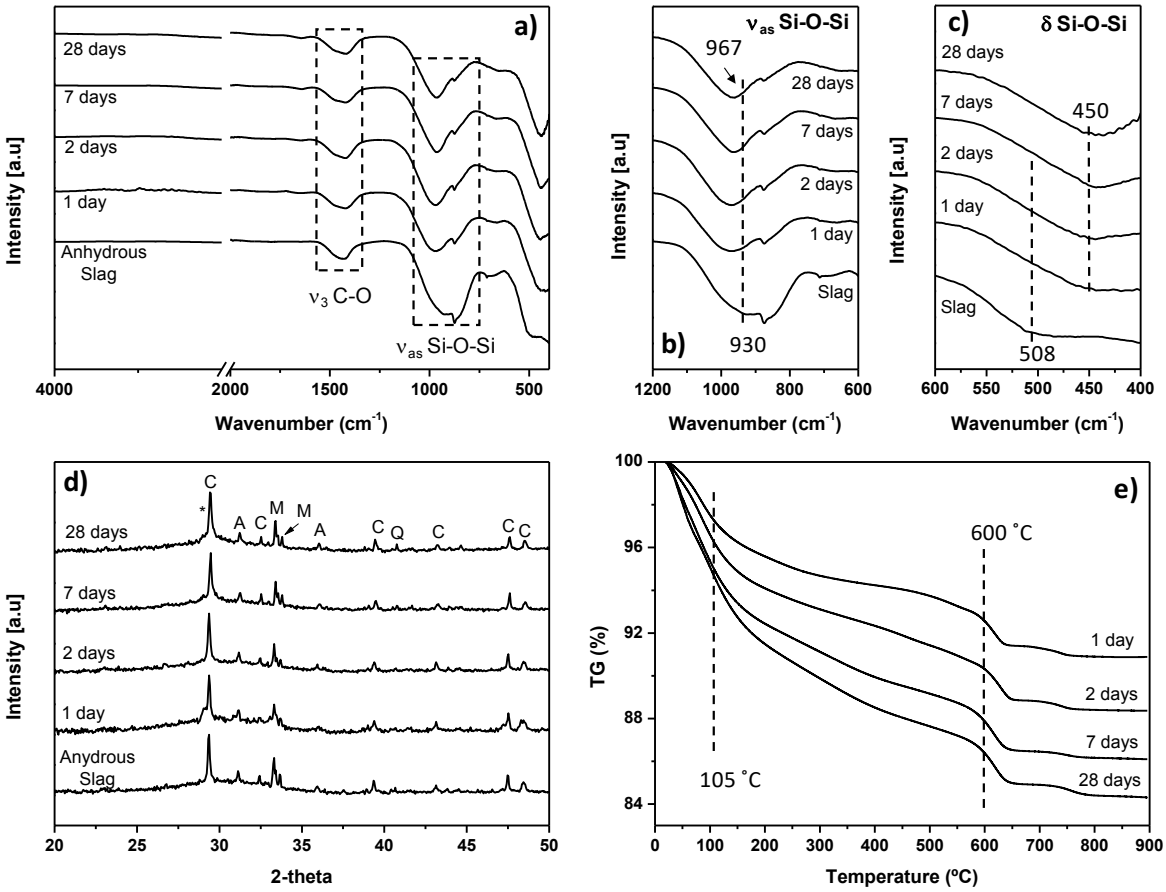

Figure 1. Determination of the blast furnace slag and the main reaction products at 1, 2, 7 and 28 days by FTIR, XRD and TG. **a)** FTIR spectra of the anhydrous blast furnace slag and AAS pastes; **b)** main absorption band associated to Si-O-Si in the range 600-1200 cm^{-1}. There is a shift of the main absorption band from 930 to 967 cm^{-1}, indicative of the formation of C-A-S-H gel (rich in silicon); **c)** absorption band associated to δ Si-O-Si. There is a FTIR shift towards lower wavenumbers, indicative of the formation of the C-A-S-H gel; **d)** XRD patterns for the anhydrous blast furnace slag and AAS pastes. The main phases present are: calcite ($CaCO_3$, C), akermanite ($Ca_2Mg(Si_2O_7)$, A), mullite (M) and quartz (SiO_2, Q). In addition, the main reaction product is the C-A-S-H gel (*) located at 2θ values in the same region of the main calcite diffraction peak; **e)** TG analysis of AAS pastes with the mass losses (%) evolution vs. temperature up to 900 ºC.

The diffractogram of the anhydrous blast furnace slag is shown in Figure 1d. A small amorphous halo with a maximum around 2θ = 30-32º can be observed. This halo coincides with the region in which the characteristic diffraction peaks of akermanite appear ($Ca_2Mg(Si_2O_7)$), at values close to 2θ = 31.1º, 28.9º and 51.8º, which constitutes a

priority phase of the slag. In addition, it is also possible to distinguish crystalline diffraction peaks attributed to the presence of quartz (2θ = 21.8º, 27.7º and 40.8º), calcite (2θ = 29.4º, 47.4º and 48.5º) and some diffraction peaks characteristic of the presence of mullite, due to the concentration of aluminum in the slag. By using the XRD technique, it is possible to observe the formation of the main reaction product, the C-A-S-H gel similarly as it was shown by FTIR. However, being an amorphous product (lower structural order) it is very complex to accurately detect it by XRD and also, the main diffraction peak overlap the most intense one of the calcite ($CaCO_3$). As consequence, XRD is not enough suitable technique for determining the amount of C-A-S-H gel at each age. Accordingly other technique such as thermogravimetry analysis (TG) are usually required [43].

The mass losses observed during the thermal treatment of the alkali activated slag are associated with the chemically combined water that it is proportional to the amount of reaction products formed (TG curve between 105-600ºC). Therefore, as the mass losses are higher, higher is the reaction degree of the slag. Table 2 shows the values of mass losses obtained from TG curves between 105-600ºC for the different study ages (1, 2, 7 and 28 days) (see Figure 1e). However, this data fails to provide the degree of reaction for the pastes and result as relative or comparative data. The water is eliminated in a generalized way throughout the range of temperatures as indicative of the amorphous nature of the formed gel. In this way, the water can occupy multiple places within the amorphous structure of the gel including from bonds with the different cations involved in the gel, to interposition places. As consequence, just considering the water in a defined interval for quantification of gel formation would represent an underestimation of such reaction product.

Table 2. Mass losses by TG between 105-600 ºC

Temperature (ºC)	1 day	2 days	7 days	28 days
105-600	4.9 %	6.3 %	7.6 %	8.9 %

In view of the obtained results, it can be observed that as the reaction time evolves, there is a greater loss of water in the interval of 105-600ºC, causing a greater degree of

reaction in the system. Therefore, this increase in the degree of reaction is indicative that the formation of the main reaction product (C-A-S-H gel) has gradually occurred.

To sum up, it can be said that conventional techniques, such as FTIR, XRD and TG provided relative information at each of the studied ages of the reaction degree of alkali-activated slag. However, some of these techniques, due to the low crystallinity of the main reaction product (C-A-S-H gel), do not provide relevant information about this reaction product, or any information related to its mechanism of formation, distribution throughout the sample, carbonation processes, etc. That is why we must resort to more sophisticated techniques, such as the case of NMR ^{29}Si and ^{27}Al, BSEM/EDX, TEM or through the use of Confocal Raman Microscopy (CRM). Of all of them, the use of CRM allows us to combine the structure and microstructure evolution of the pastes during the process of alkaline activation.

3.2. Confocal Raman Microscopy: new approach to anhydrous slag and reaction products

The Raman spectrum for the anhydrous slag is shown in Figure 2a in which different phase contributed. The presence of different phases to the average Raman spectrum of the main phases is present in Figure 2c. A weak and broad Raman band at ca. 885 cm^{-1} appears in the average spectrum. It is attributed to the symmetric stretching of Si-O-Si, v_1, of mullite phase present in the anhydrous slag [44]. Another important phase contribution to the Raman spectrum are Raman bands located at 666 cm^{-1} and 911 cm^{-1} attributed to the presence of the crystalline phase akermanite ($Ca_2Mg(Si_2O_7)$). In addition, there are Raman bands observed in the regions of 350-500 cm^{-1} and 400-600 cm^{-1} [45], which are generally attributed to v_2-type internal deformations and v_4-type asymmetric bending vibrations of SiO_4 tetrahedra, respectively [31]. An intense and narrow Raman band around ca. 1096 cm^{-1} and a less intense Raman band at ca. 283 cm^{-1} can be seen, both attributed to the presence of calcite [33].

Figure 2b shows the main Raman spectrum attributed to the commercial sodium silicate solution. There are four well-distinguished zones in the Raman spectrum of the solution: a Raman band located at ca. 525 cm^{-1} associated with the stretching modes of Si-O-Si (Q^3), a Raman band at ca. 1041 cm^{-1} attributed to the symmetric stretching of Q^3 (Q^3-SS), a Raman band at ca. 1647 cm^{-1} due to the bending vibrations of water and a very wide and intense Raman band at ca. 3400 cm^{-1} associated to the stretching vibrations of OH^- groups.

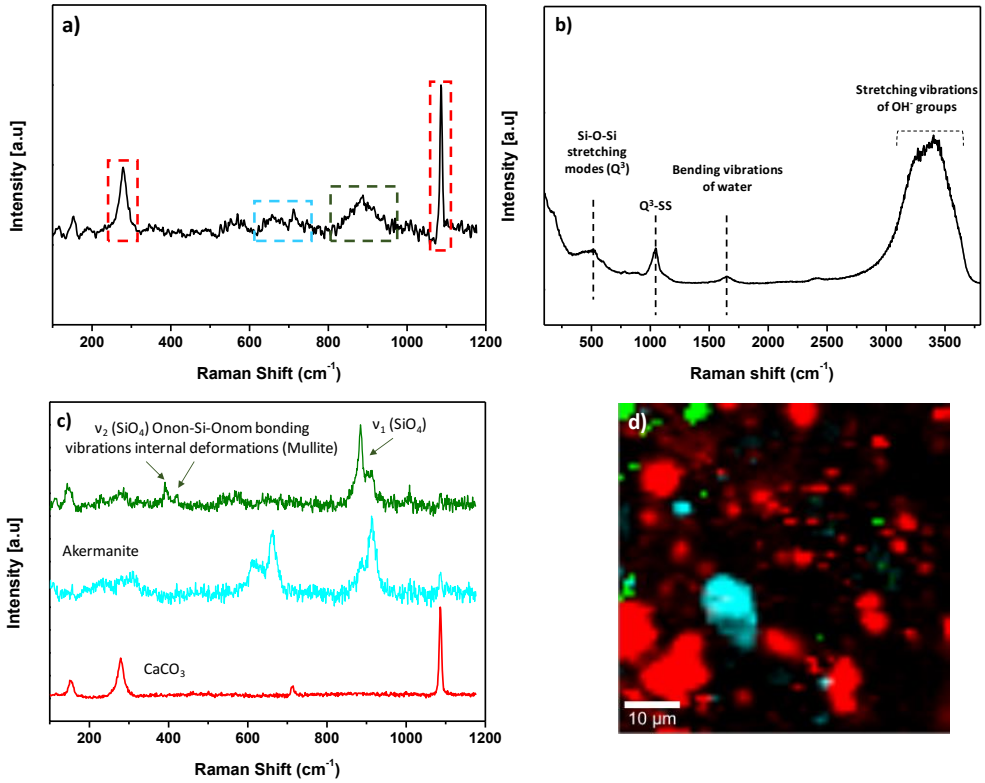

Figure 2. a) Average Raman spectrum of the anhydrous blast furnace slag; **b)** Average Raman spectrum of sodium silicate solution (waterglass solution); **c)** average Raman spectra of the main phases present in the anhydrous blast furnace slag: calcium carbonate ($CaCO_3$ in red), akermanite ($Ca_2Mg(Si_2O_7)$, in cyan) and the symmetric stretching bonds of SiO_4 from slag, in green; **d)** Surface Raman image (60x60 μm^2, integration time of 1.0 s and 60x60 pixels) by CRM of the anhydrous blast furnace slag used in this study. The main phases present in the blast furnace slag are: $CaCO_3$ in red, akermanite ($Ca_2Mg(Si_2O_7)$) in cyan and the symmetric stretching bonds of SiO_4 (v_1 Si-O-Si) of the anhydrous slag and for the presence of mullite, in green. The boxes represent the different regions of the sample where the analysis has been made.

In addition of the occurrence of different phases in the average Raman spectrum, CRM provides a microstructural view of the phase distribution. Figure 2d shows the distribution of the main observed phases signaled by their assigned color. The average particle size of the slag is d_{50} = 19 µm and due to the confocality of the system, 0.7 µm, only a portion of the sample is located at the focal plane. Therefore, the figure 2d shows the main presence of $CaCO_3$ in red with particle size lower than 10 µm, which represent a portion of the particles. The presence of carbonates in the sample is due to the easy carbonation that the slag presents on the surface due to the CO_2 action in contact with calcium. In addition, located presence of akermanite ($Ca_2Mg(Si_2O_7)$) in cyan and the symmetric stretching bonds of SiO_4 (ν_1 Si-O-Si) of the mullite from anhydrous slag, in green, are also detected.

Figure 3 shows the average Raman spectra of the anhydrous blast furnace slag and the alkali-activated slag with the sodium silicate at the different hydration ages (1, 2, 7 and 28 days). When the slag is activated with the solution of sodium silicate (or waterglass solution), the Raman bands attributed to the presence of the main phases of the anhydrous slag are observed and, in addition, new Raman bands are distinguished associated with the formation of the main products of reaction. It is observed how at approximately ca. 673 cm^{-1} the appearance of a new Raman band associated with the formation of the main reaction product is seen: C-A-S-H gel. This Raman band is assigned to Q^2 Si-O-Si symmetric bending vibrations [31]. The C-A-S-H gel is characterized as a reaction product with low crystallinity and its detection by XRD is quite complex. However, under the CRM measurement conditions established (532 nm excitation laser; a 100X objective lens, N.A. 0.95; 20 mW laser power, integration time per pixel was 1.0s) it is possible to detect relevant signal for each age. For the treatment of the results obtained by Confocal Raman microscopy, "cosmic rays remove" (CRR) and "background subtraction" (BSub) were performed [46]. At the age of 1 and 2 days of activation, a little more defined Raman band around ca. 673 cm^{-1} is observed in the average spectrum (see Figure 3b) than at more advanced ages (7 and 28 days), indicating that it has formed greater amount of C-A-S-H gel at advanced ages. Moreover, the intensity of that band coincides with the presence of the anhydrous phase of the slag (akermanite, $Ca_2Mg(Si_2O_7)$) which has a main band at ca. 666 cm^{-1} (see Figure 2c). As the reaction time evolves, a greater amount of C-A-S-H gel is generated in the system, being at the ages of 7 and 28 days where the greatest amount of gel is

observed, both in the average spectra (see Figure 3b) and in the different micrographs obtained (see Figure 3c).

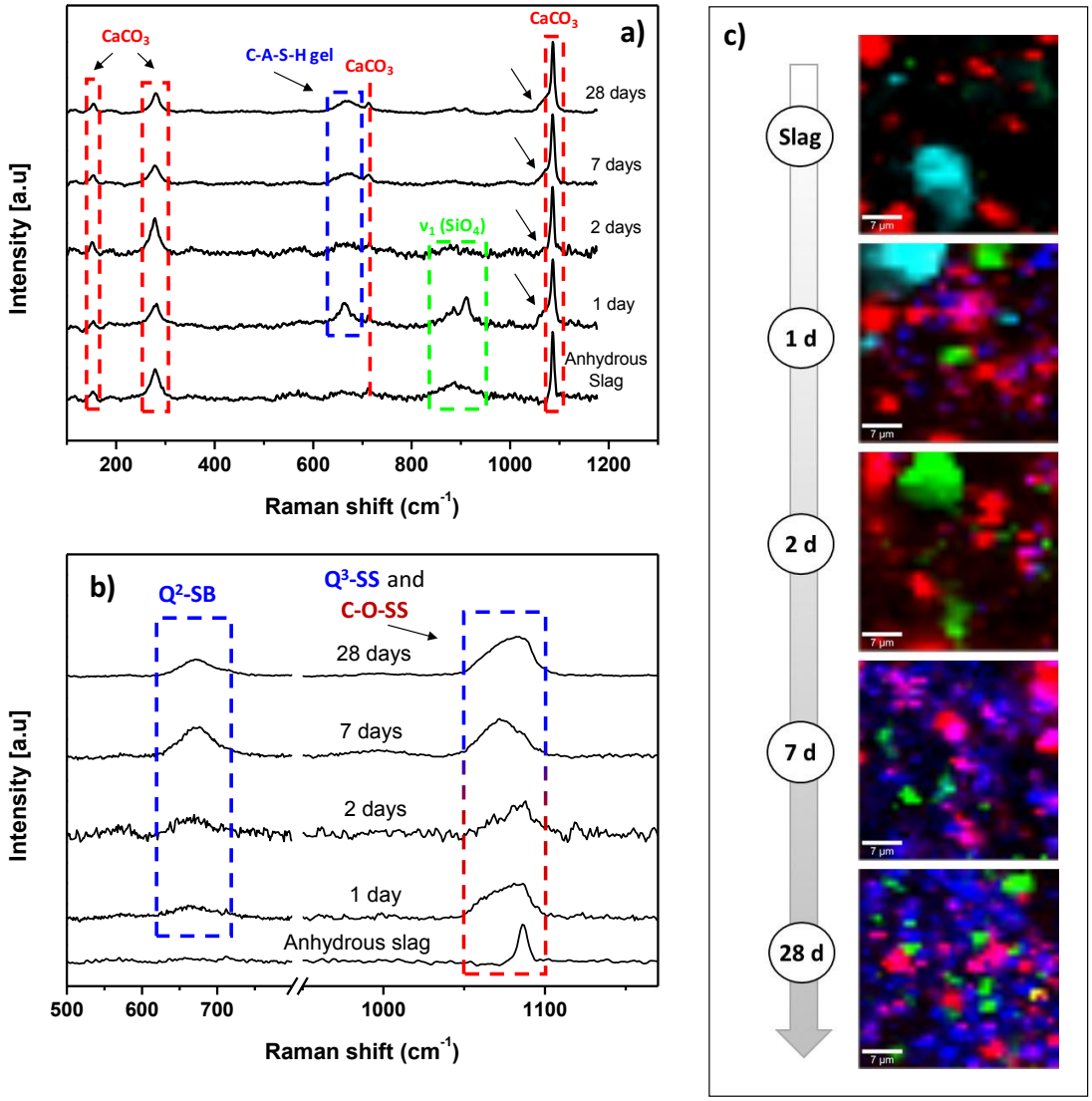

Figure 3. a) Average Raman spectra of the anhydrous blast furnace slag and the alkali-activated slag at different ages (1, 2, 7 and 28 days) obtained by Confocal Raman Microscopy (CRM). **b)** Average Raman spectra of region where C-A-S-H gel Raman bands are located at different activation times. The main Raman band of the C-A-S-H gel is located ca. 666 cm^{-1}, attributed to Si-O-Si symmetric bending Q^2 (Q^2-SB); and a Raman band ca. 1040 cm^{-1}, associated to the symmetric stretching of Q^3 (Q^3-SS) and symmetric stretching of O-C-O group in $CaCO_3$ precipitates (C-O-SS); **c)** Raman images by CRM (35x35 µm, integration time of 1.0 s and 35x35

pixels) of the evolution of the main phases of anhydrous slag (akermanite, in cyan and the symmetric stretching bonds of SiO_4 from slag, in green), calcite ($CaCO_3$, in red) and the formation of the main reaction product in this system (C-A-S-H gel, in blue).

Another aspect to be highlighted from the results of CRM is the presence of carbonates in the samples ($CaCO_3$). In the average Raman spectrum of the anhydrous slag, the presence of a calcite-like crystalline carbonate is unequivocal. The Raman spectrum of calcite possesses different Raman modes: Raman modes at ca. 180 and 280 cm^{-1} are due to the relative translations between the cation and anionic groups; at ca. 711 cm^{-1} the vibration mode v_4 is attributed to symmetric CO_3 deformation; and at ca. 1085 cm^{-1} the vibration mode v_1 that corresponds to the symmetric stretching of O-C-O group in $CaCO_3$ precipitates such as calcite [25,33,47]. However, these Raman bands as a signal of the presence of calcite in the slag remain practically unaltered during the alkaline activation with sodium silicate. From the beginning of the reaction, there are regions of slag that are partially carbonated, especially these regions are revealed at the surface of the reaction product due their high crystallinity and opacity. In addition, with the reaction time, as the calcium of the slag dissolves in the silicates solution, a calcium enrichment of the solution occurs and therefore the appearance of calcite it is also promoted by the available atmospheric CO_2 [48,49].

As regards the main phase of the silicates, either from the solid precursor (slag) or from the liquid precursor (sodium silicate or waterglass solution), are also maintained throughout the hydration, being the source of silicates for the formation of the C-A-S-H gel. However, this behavior does not account for the akermanite presence, which it is only detected in the anhydrous slag and for 1-2 days of activation. Moreover, the presence of akermanite at early ages of reaction difficult the detection of the C-A-S-H gel, since the Raman bands of both compounds overlap in the same spectral region. The large presence of well crystallize akermanite in early hours enlarges their Raman signal in comparison to the low Raman signal of the C-A-S-H gel itself.

What happens with the formation of the C-A-S-H gel? At the first activation ages (1 and 2 days) the appearance of the main reaction product is hardly observed. As the activation process evolves the precipitation of the gel occurs in the solution (see Figure 3) and the growth of the gel could occur in a different way than the growth of the C-S-

H gel in a conventional Portland cement. In a Portland cement system, C-S-H gel growths around the C_3S particles forming layers [32]. However, in the alkali-activated slag systems the growth of the C-A-S-H gel is randomly attained. At early ages, the hydration products formed in the space between the slag grains originally occupied by alkaline solution, indicating that its formation occurs through a dissolution and precipitation mechanism. Other techniques such as SEM are unable to detect the main reaction products when the activator is a waterglass solution because of the homogeneous and amorphous appearance of the C-A-S-H gel. By the contrary, with the use of CRM it is possible to determine the growth and evolution of C-A-S-H gel.

Figure 3b shows the main Raman band of the C-A-S-H gel that appears at ca. 666 cm^{-1} [31]. In addition, there are other important Raman bands in the regions of 350-500 cm^{-1} and 400-600 cm^{-1} generally attributed to v_2-type internal deformation and v_4-type asymmetric bending vibrations of SiO_4 tetrahedra, respectively [31]. However, in the average Raman spectrum it is possible to observe how the Raman band that appears ca. 1080 cm^{-1} widens with the activation time. In addition to presence of calcite there is a coexisting Raman band attributed to symmetric stretching of Q^3, due to the polymerization of the C-A-S-H gel chains. Moreover, in this region of the Raman spectrum the main Raman bands of the sodium silicate solutions also contributes to its widening (see Figure 3b).

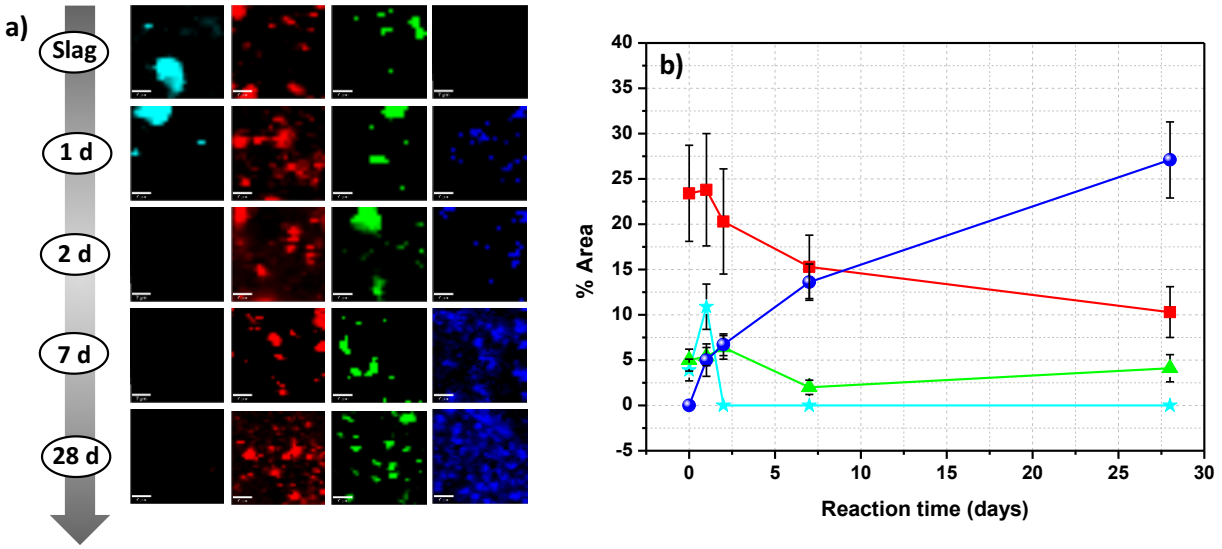

Figure 4. a) Raman images by CRM (35x35 μm^2, integration time of 1.0 s and 35x35 pixels) of the evolution of the main phases present in the alkali-activated slag at different ages (1, 2, 7 and 28

days): akermanite (in cyan), calcite ($CaCO_3$, in red), the symmetric stretching bonds of SiO_4 from slag (in green), and the presence of C-A-S-H gel (in blue); **b)** semi-quantitative determination of the presence of the main phases present during the alkali-activation of blast furnace slag: akermanite (in cyan), calcite (in red), the symmetric stretching bonds of SiO_4 (in green) and the C-A-S-H gel (in blue).

From a semi-quantitative point of view, the use of CRM allows to obtain more detailed information on each of the phases present in the alkali-activated system. To obtain semi-quantitative information an area of the material of35x35 μm^2 is analyzed. As the laser illuminates a fixed depth, 0.7 µm, due the confocality of CRM, the area is a comparable unit of measurement. Additionally, the criterion to validate the presence of a phase in each pixel is defined as an intensity of 5 times greater than the background noise in that spectral region [33,46]. To generate the image corresponding to each of the phases analyzed, the area under the most intense Raman bands was calculated. The spectra were not normalized, but in order to compare the sweeps at different times, before each of them, the laser power was adjusted to 20 mW with a potentiometer, so that all were taken under the same conditions (power, integration time, size of scanned area and number of points per scan).

Figure 4 shows the phase percentage evolution during the activation time of anhydrous slag with the sodium silicate solution. On the other hand, with regard to carbonate content as the reaction with the sodium silicate occurs and the slag dissolves, said carbonates dissolve too. In addition to the starting carbonates, new carbonates appear in regions close to the formation of the C-A-S-H gel, as indicative that the C-A-S-H gel itself is susceptible to being carbonated.

As previously mentioned, the formation of the C-A-S-H gel evolves with the activation time, and this can be corroborated by Raman semi-quantification (see Figure 4). Although there is also a high percentage of carbonates in the system that can inhibit the Raman signal related to the C-A-S-H gel because they are more crystalline, the use of the CRM technique gives a high degree of reliability in the semi-quantification of the gel the different ages. Unlike the semi-quantification obtained by DTA/TG, which is established from the water loss associated with the C-A-S-H gel in a temperature range between 105-600ºC, by means of CRM the amount of C-A-S-H gel formed from first ages of reaction is in situ without the need of destructive thermal treatment. When working at room temperature, the amount of water lost related to the gel (water

chemically combined in the gel) is not provide, but the information obtained is much more real and concise of all the composition present in said amorphous material. The comparative data of C-A-S-H gel obtained by using DTA/TG or CRM is shown in Figure 5. A higher percentage of C-A-S-H gel is obtained from the CRM analysis that account for a higher degree of reaction as above stated. By CRM a greater relative increase of C-A-S-H with time for older ages than for early ages, while in DTA/TG analyses the increase is more relevant for early ages. It is important to specify that the data obtained by DTA/TG are % by weight and those obtained by CRM in % by volume (surface), obtained after counting the number of pixels by the proportion within each pixel. Therefore, it is a relevant aspect to compare how gel evolves whit each characterization technique. In addition, it is worth to note that by CRM it is possible to microstructurally determine the area where C-A-S-H gel in present. Thus, the C-A-S-H gel determined by CRM is more than three times higher than the percentage shown by ATD/TG. This value is more realistic and it is associated with the presence of large amount of C-A-S-H gel despite their low crystallinity.

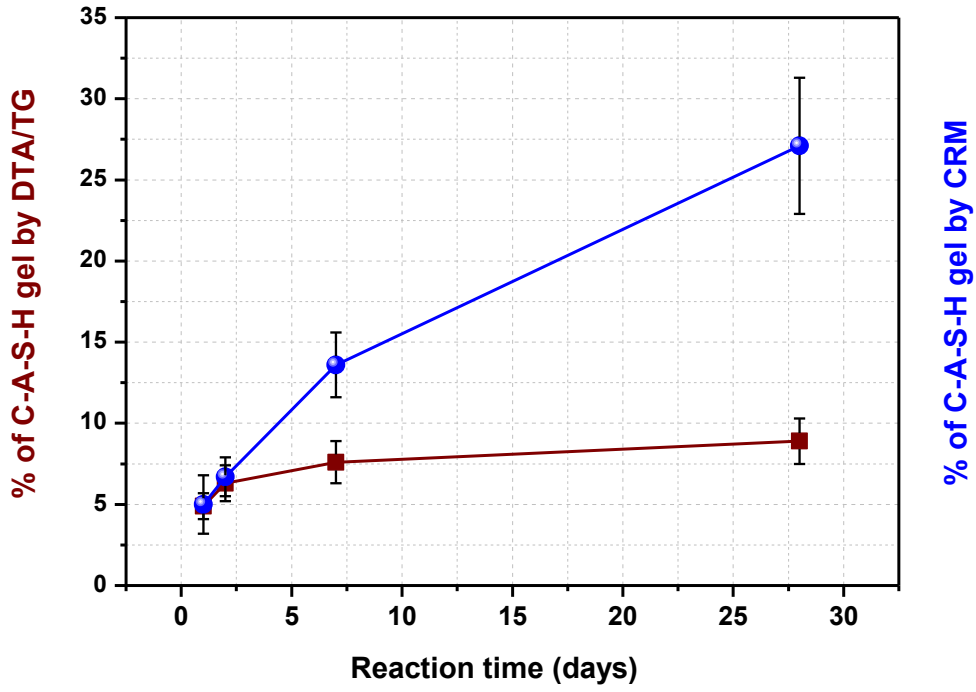

Figure 5. Semi-quantitative determination of the presence of C-A-S-H gel determined by Confocal Raman Microscopy (% by volume) and by DTA/TG (% by weight).

Conclusions

The feasibility to use Confocal Raman Microscopy (CRM) as new characterization technique in alkali-activated materials has been proven. The results obtained by conventional characterization techniques (FTIR, XRD or DTA/TG) allow obtaining information about the main components existing in the slag, and also, it provides information about the main reaction product: C-A-S-H gel. However, due to the slightly crystalline nature of the C-A-S-H gel, techniques such as XRD are not reliable at all to obtain such detailed information on the C-A-S-H gel. To obtain information on the degree of reaction of the activated pastes with a sodium silicate solution, it is possible to resort to the DTA/TG technique, where from the loss or water in the 105-600ºC temperature range associated with the chemically bound water of the C-A-S-H gel, the evolution of the gel can be known. However, the use of this technique gives and underestimation on the degree of reaction based on the water eliminated, and no more detailed information is obtained on the composition or morphology of the C-A-S-H gel.

The use of CRM, due to the combination of the high spectral resolution Raman spectroscopy with a high spatial resolution of the Confocal Microscopy, shows the presence and distribution of the main phases present in the alkali-activated system at different ages. The microstructure location of the C-A-S-H gel, despite its low crystallinity, allows obtaining more detailed information on the slag hydration at different ages, in addition to being able to use this technique as a much more complete semi-quantification technique from a compositional point of view. In addition, the use of CRM has corroborated how the growth of the C-A-S-H gel is different to the growth of a C-S-H gel in OPC systems. The growth of C-A-S-H gel occurs randomly in the medium, always in regions where there is dissolved calcium from the slag.

The use of the CRM opens a new alternative of microstructural characterization in the alkali-activated material or geopolymers, allowing to know the mechanisms involved during the activation, generating of new phases, and possibly, facilitate the understanding of some phenomena related to the durability of these systems against carbonation, freeze-thaw or by attacks with sulphates or chlorides.

Acknowledgements

This work was supported by the Spanish Ministry of Economy and Competitiveness through the Project MAT-2017-86450-C4-1-R and Spanish National Research Council Project NANOMIND 201560E068. Dr. M. Torres-Carrasco is also indebted to MINECO for a postdoctoral fellowship "Juan de la Cierva-Formación" (ref: FJCI-2016-28488). In addition, O. Mikhailova enjoyed a pre-doctoral fellowship with specific junior project FAST-J-18-5568 from the Brno University of Technology (Czech Republic) for internship in Spain.

References

[1] R.M. Andrew, Global CO_2 emissions from cement production, Earth Syst. Sci. Data Discuss. (2017) 1–52.

[2] M. Ba-Shammakh, H. Caruso, A. Elkamel, E. Croiset, P.L. Douglas, Analysis and optimization of carbon dioxide emission mitigation options in the cement industry, Am. J. Environ. Sci. 4 (2008) 482–490.

[3] S. A Bernal, R.M. De Gutierrez, E.D. Rodríguez, Alkali-activated materials : cementing a sustainable future, Ing. Y Compet. 15 (2013) 211–223.

[4] J.L. Provis, A. Palomo, C. Shi, Advances in understanding alkali-activated materials, Cem. Concr. Res. 78 (2015) 110–125.

[5] C. Shi, P. Krivenko, D. Roy, Alkali-Activated Cements and Concretes, Taylor and Francis, London and New York, 2006.

[6] T. Bakharev, J.G. Sanjayan, Y.-B. Cheng, Alkali activation of Australian slag cements, Cem. Concr. Res. 29 (1999) 113–120.

[7] A. Fernández-Jiménez, J.G. Palomo, F. Puertas, Alkali-activated slag mortars Mechanical strength behaviour, Cem. Concr. Compos. 29 (1999) 1313–1321.

[8] H. Kukko, R. Mannonen, Chemical and mechanical properties of alkali-activated blast furnace slag (F-concrete), Nord. Concr. Res. 1 (1983) 1–16.

[9] A. Palomo, M.T. Blanco-Varela, M.L. Granizo, F. Puertas, T. Vazquez, M.W. Grutzeck, Chemical stability of cementitious materials based on metakaolin, Cem. Concr. Res. 29 (1999) 997–1004.

[10] A. Khmiri, M. Chaabouni, B. Samet, Chemical behaviour of ground waste glass when used as partial cement replacement in mortars, Constr. Build. Mater. 44 (2013) 74–80.

[11] M. Torres-Carrasco, M. Tognonvi, A. Tagnit-Hamou, F. Puertas, Durability of Alkali-Activated Slag Concretes Prepared using waste glass as Alternative activator, ACI. 112 (2015) 791–800.

[12] A. Cornejo, C. Leiva, L.F. Vilches, Properties of fly ash and metakaolín based

geopolymer panels under fire resistance tests, Mater. Construcción. 65 (2015) e059.

[13] C. Shi, Another look at the rapid chloride permeability test (ASTM C1202 or ASSHTO T277), in: FHWA Resour. Cent., Baltimore, 2003.

[14] C. Shi, P. Xie, Interface between cement paste and quartz sand in alkali-activated slag mortars, Cem. Concr. Res. 28 (1998) 887–896.

[15] A.R. Brough, A. Atkinson, Automated identification of the aggregate-paste interfacial transition zone in mortars of silica sand with Portland or alkali-activated slag cement paste, Cem. Concr. Res. 30 (2000) 849–854.

[16] I.G. Richardson, The calcium silicate hydrates, Cem. Concr. Res. 38 (2008) 137–158.

[17] P. Duxson, A. Fernández-Jiménez, J.L. Provis, G.C. Lukey, a. Palomo, J.S.J. Deventer, Geopolymer technology: the current state of the art, J. Mater. Sci. 42 (2006) 2917–2933.

[18] J.L. Provis, J.S.J. van Deventer, Alkali-Activated Materials. State of the Art Report, RILEM TC 224-AAM, 2014.

[19] A. Palomo, P. Krivenko, E. Kavalerova, O. Maltseva, A review on alkaline activation : new analytical perspectives, Mater. Construcción. 64 (2014).

[20] F. Puertas, M. Palacios, H. Manzano, J.S. Dolado, a. Rico, J. Rodríguez, A model for the C-A-S-H gel formed in alkali-activated slag cements, J. Eur. Ceram. Soc. 31 (2011) 2043–2056.

[21] V.O. Özçelik, C.E. White, Nanoscale Charge-Balancing Mechanism in Alkali-Substituted Calcium-Silicate-Hydrate Gels, J. Phys. Chem. Lett. 7 (2016) 5266–5272.

[22] M. Ben Haha, B. Lothenbach, G. Le Saout, F. Winnefeld, Influence of slag chemistry on the hydration of alkali-activated blast-furnace slag — Part II: Effect of Al2O3, Cem. Concr. Res. 42 (2012) 74–83.

[23] Z. Pan, Z. Tao, Y.F. Cao, R. Wuhrer, T. Murphy, Compressive strength and microstructure of alkali-activated fly ash/slag binders at high temperature, Cem. Concr. Compos. 86 (2018) 9–18.

[24] I.G. Richardson, L. Black, J. Skibsted, R.J. Kirkpatrick, Characterisation of cement hydrate phases by TEM, NMR and Raman spectroscopy, Adv. Cem. Res. 22 (2010) 233–248.

[25] R.J. Kirkpatrick, J.L. Yarger, P.F. McMillan, Y. Ping, X. Cong, Raman spectroscopy of C-S-H, tobermorite, and jennite, Adv. Cem. Based Mater. 5 (1997) 93–99.

[26] L. Black, Raman Spectroscopy of cementitious materials, in: J. Yarwood, R. Douthwaite, S. Duckett (Eds.), Spectrosc. Prop. Inorg. Organomet. Compd., Royal Society of Chemistry, 2009.

[27] J. Bensted, S. Prakash Varma, Some applications of infrared and Raman spectroscopy in cement chemistry. Part 2: Portland cements and its constituents, Cem. Technol. 5 (1974) 378–382.

[28] D. Torréns-Martín, L. Fernández-Carrasco, S. Martínez-Ramírez, J. Ibáñez, L. Artús, T. Matschei, Raman spectroscopy of anhydrous and hydrated calcium aluminates and sulfoaluminates, J. Am. Ceram. Soc. 96 (2013) 3589–3595.

[29] S.S. Potgieter-Vermaak, J.H. Potgieter, M. Belleil, F. Deweerdt, R. Van Grieken, The application of Raman spectrometry to the investigation of cement: Part II: A micro-Raman study of OPC, slag and fly ash, Cem. Concr. Res. 36 (2006) 663–670.

[30] S.N. Ghosh, S.K. Handoo, Infrared and Raman spectral studies in cement and concrete (review), Cem. Concr. Res. 10 (1980) 771–782.

[31] S. Ortaboy, J. Li, G. Geng, R.J. Myers, P.J.M. Monteiro, R. Maboudian, C. Carraro, Effects of CO2 and temperature on the structure and chemistry of C–(A–)S–H investigated by Raman spectroscopy, RSC Adv. 7 (2017) 48925–48933.

[32] J. Higl, M. Köhler, M. Lindén, Confocal Raman microscopy as a non-destructive tool to study microstructure of hydrating cementitious materials, Cem. Concr. Res. 88 (2016) 136–143.

[33] M. Torres-carrasco, A. Campo, M.A. De Rubia, E. Reyes, A. Moragues, J.F. Fernández, New insights in weathering analysis of anhydrous cements by using high spectral and spatial resolution Confocal Raman Microscopy, Cem. Concr. Res. 100 (2017) 119–128.

[34] T. Schmid, P. Dariz, Determination and imaging of binder remnants and aggregates in historic cement stone by Raman microscopy, J. Raman Spectrosc. 44 (2013) 882–891.

[35] K. Scrivener, R. Snellings, B. Lothenbach, A Practical Guide to Microstructural Analysis of Cementitious Materials, Taylor and Francis, 2016.

[36] J.A. Gadsden, Infrared spectra of minerals and related inorganic compounds, Butterworth & CO Publishers, London, 1975.

[37] M. Palacios, F. Puertas, Effect of Carbonation on Alkali-Activated Slag Paste, J. Am. Ceram. Soc. 89 (2006) 3211–3221.

[38] S.S. Potgieter-Vermaak, J.H. Potgieter, R. Van Grieken, The application of Raman spectrometry to investigate and characterize cement, Part I: A review, Cem. Concr. Res. 36 (2006) 656–662.

[39] D.H. Chu, M. Vinoba, M. Bhagiyalakshmi, I.H. Baek, S.C. Nam, Y. Yoon, S.H. Kim, S.K. Jeong, CO_2 mineralization into different polymorphs of $CaCO_3$ using an aqueous-CO_2 system, RSC Adv. 3 (2013) 21722–21729.

[40] F. Puertas, A. Fernández-Jiménez, M.. Blanco-Varela, Pore solution in alkali-activated slag cement pastes. Relation to the composition and structure of calcium silicate hydrate, Cem. Concr. Res. 34 (2004) 139–148.

[41] I. Garcia-Lodeiro, E. Aparicio-Rebollo, A. Fernández-Jimenez, A. Palomo, Effect of calcium on the alkaline activation of aluminosilicate glass, Ceram. Int. 42 (2016) 7697–7707.

[42] I. García-Lodeiro, A. Fernández-Jiménez, M.T. Blanco, A. Palomo, FTIR study of the sol-gel synthesis of cementitious gels: C-S-H and N-A-S-H, J. Sol-Gel Sci. Technol. 45 (2008) 63–72.

[43] A. Fernández-Jiménez, F. Puertas, Cementos de escorias activados alcalinamente. Determinación del grado de reacción Alkaline activated slag cements . Determination of reaction degree, Mater. Construcción. 51 (2001) 53–66.

[44] N. Bost, S. Duraipandian, G. Guimbretière, J. Poirier, Raman spectra of synthetic and natural mullite, Vib. Spectrosc. 82 (2016) 50–52.

[45] http://rruff.info/, (n.d.).

[46] T. Dieing, O. Hollricher, J. Toporski, Confocal Raman Microscopy, Springer, 2010.

[47] S. Gunasekaran, G. Anbalagan, S. Pandi, Raman and infrared spectra of carbonates of calcite structure, J. Raman Spectrosc. 37 (2006) 892–899.

[48] S.A. Bernal, R. San Nicolas, J.L. Provis, R. Mejía de Gutiérrez, J.S.J. van Deventer, Natural carbonation of aged alkali-activated slag concretes, Mater. Struct. 47 (2014) 693–707.

[49] S.A. Bernal, J. Provis, B. Walkley, R. San Nicolas, J. Gehman, D. Brice, A. Kilcullen, P. Duxson, J.S.J. Van Deventer, Gel nanostructure in alkali-activated binders based on slag and fl y ash , and effects of accelerated carbonation, Cem. Concr. Res. 53 (2013) 127–144.